Transition from saliva droplets to solid aerosols in the context of COVID-19 spreading

Mehdi Stiti, Guillaume Castanet, Andrew Corber, Marcus Alden, Edouard Berrocal

Transition from saliva droplets to solid aerosols in the context of COVID-19 spreading

Mehdi Stiti [a,*], Guilaume Castanet [b], Andrew Corber [c], Marcus Alden [a], Edouard Berrocal [a,**]

[a] Division of Combustion Physics, Department of Physics, Lund University, Lund, Sweden
[b] Université de Lorraine, CNRS, LEMTA, Nancy, France
[c] Aerospace Research Centre, National Research Council of Canada, Ottawa, Canada

Keywords:
COVID-19
Airborne transmission
Saliva evaporation
Droplets
Aerosols

A B S T R A C T

To control the evolution of a pandemic such as COVID-19, knowing the conditions under which the pathogen is being transmitted represents a critical issue, especially when implementing protection strategies such as social distancing and wearing face masks. For viruses and bacteria that spread via airborne and/or droplet pathways, this requires understanding how saliva droplets evolve over time after their expulsion by speaking or coughing. Within this context, the transition from saliva droplets to solid residues, due to water evaporation, is studied here both experimentally, considering the saliva from 5 men and 5 women, and via numerical modeling to accurately predict the dynamics of this process. The model assumes saliva to be a binary water/salt mixture and is validated against experimental results using saliva droplets that are suspended in an ultrasound levitator. We demonstrate that droplets with an initial diameter smaller than 21 μm will produce a solid residue that would be considered an aerosol of <5 μm diameter in less than 2 s (for any relative humidity less than 80% and/or any temperature greater than 20°C). Finally, the model developed here accounts for the influence of the saliva composition, relative humidity and ambient temperature on droplet drying. Thus, the travel distance prior to becoming a solid residue can be deduced. We found that saliva droplets of initial size below 80 μm, which corresponds to the vast majority of speech and cough droplets, will become solid residues prior to touching the ground when expelled from a height of 160 cm.

Virus transmission can occur by way of three different modes. The first consists of direct contact with an infectious person, such as touching of the face. The second, involves particles being ejected when breathing, speaking or coughing, that travel via the air from the host to a susceptible mucosal surface of another person. The last transmission pathway can occur when saliva droplets that contains the virus are deposited on surfaces or objects, known as fomites, which are then transferred via touch. It has recently been established that the transmission of COVID-19 by fomites, has a lower probability in comparison to the two other modes (Goldman, 2020; Lewis, 2021). If direct contact from person to person is avoided, then the most important transmission mode is via airway, from particles being emitted when breathing, speaking, coughing and sneezing. In that case, the size of the particles being ejected is a critical parameter. Researchers in the field of medicine usually divide the particles found in human respiratory emissions into two categories, “aerosols” and “droplets” (Jayaweera et al., 2020). The defining difference between them being that aerosols are smaller than 5 μm in diameter, can hang in the air indefinitely and diffuse deep into the lung tissue when inhaled. While this definition has been adopted by the Centre for Disease Control (CDC) and the World Health Organization (WHO), it differs from what is commonly used in the field of atmospheric aerosols science where particles and droplets up to several tens of microns (e.g. cloud droplet) are still considered to be aerosols (Boucher, 2015). Several studies have been conducted since the outbreak of COVID-19 in order to obtain information on the transport of droplets in indoor and outdoor environments (Dbouk and Drikakis, 2020; Blocken et al., Marchal; Feng et al., 2020; Páscoa, 2020; Wang et al., 2020; Chaudhuri et al., 2020). In an open space setting, Dbouk et al. (Dbouk and Drikakis, 2020) showed that droplets could travel distances greater than 6 m with a wind speed varying from 1.1 m/s to 4.2 m/s, while Blocken et al. (Blocken et al., Marchal) highlighted the presence of droplets in the wake of a runner. Shao et al. (2021) showed

* Corresponding author.
** Corresponding author.
E-mail addresses: mehdi.stiti@forbrf.lth.se (M. Stiti), edouard.berrocal@forbrf.lth.se (E. Berrocal).

https://doi.org/10.1016/j.envres.2021.112072
Received 24 May 2021; Received in revised form 11 August 2021; Accepted 11 September 2021
Available online 23 September 2021

that droplet clouds can propagate through the aisle of a store in just few minutes. For the case of coughing, it has been shown that the ejected droplets may contain a wide variety of pathogens including measles (Liljeroos et al., 2011) or influenza viruses (Yanet al., 2018). The distance viruses can spread via cough remains controversial with some studies indicating the range is as far as 6 m (Bourouiba, 2020; Liet al., 2020), while others claim it is only 1–2 m (Prasanna Simha and Mohan Rao, 2020). Recent studies suggest that the commonly used social distance of 1 m is insufficient, as respiratory emissions are capable of traveling much greater distances (Bourouiba, 2020; Joneset al., 2020).

The transport of saliva droplets is complex and depends on a large number of parameters including the initial droplet diameter, density and velocity, as well as the dynamic characteristics of the surrounding air. Most importantly, water evaporation from saliva droplets must also be considered as it reduces the droplet size over time, and thus affects its transport properties. As a result, the chemical composition of the droplets, as well as the relative humidity and temperature of the surrounding air, play a crucial role in the process. To accurately account for these parameters, advanced numerical modeling is necessary, which includes the adequate physics that faithfully represent the governing dynamics. The first step is then to find the appropriate properties for saliva, which is more complex than pure water. In addition to water, which represents ~99% of its mass, human saliva contains mucus, amylase, electrolytes, salt, white blood cells, epithelial cells, proteins and enzymes. These additional compounds are not volatile (Van Doremalen et al., 2020), so respiratory droplets do not completely evaporate, and small residual particles remain at the end of the evaporation process. Those residues potentially provide a means for the virus to be transported over larger distance, provided it survives the drying process (Prather et al., 2020; Lewis, 2020; Asadiet al., 2020). Arguably, accounting for the complex nature of saliva is a major modeling challenge. Thermophysical properties of saliva are poorly referenced in the literature making it difficult to apply existing evaporation models directly. A recently proposed simplification, replaces the non-volatile components by NaCl salt (Liet al., 2020; JI and Jaakko, 2013). Although the hypothesis of a binary mixture greatly simplifies the evaporation problem, the initial fraction of NaCl in the mixture has to be adjusted very carefully to obtain an evaporation rate in agreement with the experiment. This approach has been applied to a very limited number of cases to date (Liet al., 2020; JI and Jaakko, 2013), which raises questions about the most appropriate concentration of NaCl and its possible variation among individuals, or even for the same person at different times. To determine how saliva droplets evolve, heat and mass transfer inside the liquid phase also need to be carefully addressed at each time step. Previous studies (Brenn et al., 2007) on the evaporation of multi-component droplets have shown the importance of considering variable liquid properties, interspecies liquid diffusivity, as well as heat conduction and convection inside the droplet. Additionally, some mixtures need to be handled as a thermodynamically real fluids with the use of chemical activities to properly evaluate the vapor pressure at the liquid/gas interface. In the present study, the theoretical model developed for the evaporation of water/NaCl droplets is intended to address most of the effects listed above. This model is based on a quasi-steady transport process in the gas phase which allows for the evaluation of the vapor flow rate and the heat exchanged with the surrounding gas at each instant of the evaporation process (Sirignano and Edwards, 2000). To determine the initial composition of the simulated droplet, preliminary experimental measurements have been carried out on dozens of saliva droplets suspended in the air using an ultrasonic levitator. Once the water evaporation is complete, the dimension of the remaining solid residual particle is measured and compared with the initial droplet size. From these observations, the initial mass concentration of NaCl that should be used, and its variability in a population of several individuals has been estimated. Input data from these experimental findings, are inserted in the numerical model which is then used to predict the lifetime of the droplets suspended in the air under different ambient temperature and humidity conditions. Simulations are applied for two cases: First, for static droplets suspended in an ultrasonic levitator. Second, for droplets being transported in the air during a cough. In the second, the evaporation model is complemented by a description of the drop motion, including the effect of the drag force on trajectory.

1. Experimental study of saliva droplet evaporation under acoustic levitation

Measurements on saliva droplets expelled by coughing or sneezing usually consist of imaging the whole flow field using high-speed cameras (Bourouiba et al., 2014; Gupta et al., 2009). This approach allows the velocity and the number of expelled droplets to be obtained, as well as visualize their displacement over time (Roth et al., 2021). Despite the benefits of the high-temporal resolution offered by high-speed cameras, spatially resolving fast moving micrometric droplets subjected to complex surrounding air flows, and having non-linear displacements, remains a challenge. This would require developing a high-resolution imaging device capable of tracking the moving droplets over the three-dimensional space, from the mouth until water evaporation is complete and/or the droplets deposit on a surface. A simplified configuration for imaging droplets at high resolution, and studying the drying process over time, consists instead of making the droplets motionless.

A stationary single droplet can be obtained by means of either mechanical, optical or ultrasonic devices. The reliability and the accuracy of techniques with mechanical suspension of the droplet (a few mm) suffer from the influence of the needle or the wire, which affects the heat and mass transfer due to conduction and droplet surface deformation (Czerwiecet al., 2017). The use of optical trapping devices allows much smaller droplets (a few tens of μm) to be suspended in the air (Liuet al., 2016). However, the exposition of the droplets to a focused laser beam may impact and accelerate the evaporation process. The third solution is to use ultrasonic levitators. Similar to optical tracking, the approach also allows a single droplet to be held in the air without any surface contact. The advantages of ultrasonic levitation is that a large range of droplet sizes can be be suspended (from 1 mm down to 40 μm). However, the acoustic field deforms large droplets, and convection from acoustic streaming will affect evaporation. Those effects must be considered when validating numerical models. Acoustic levitation has been used in non-intrusive investigations of droplet evaporation under a wide range of conditions: the evaporation of single and multi-component droplets (Brenn et al., 2007; Yarin et al., 1999), the drying of droplets that contain solid particles in suspension (Zaitoneet al., 2006), and recently the evaporation of saliva droplets (Lieber et al., 2021).

In this article, the acoustic levitator consists of a transducer and a concave reflector. The transducer is attached to a piezoelectric crystal that vibrates at a frequency of 58 kHz (Scheme and picture of the experimental setup can be seen in Fig. S1 in the Supplementary Information). The distance between the transducer and the reflector is adjusted with a micrometer in order to maintain a standing wave, typically containing 4–6 pressure nodes. The droplet stabilizes in the acoustic field at a position slightly below a pressure node. The pressure difference between the top and the bottom of the droplet generates a force that overcomes gravity keeping the droplet suspended. This differential pressure tends to flatten the droplet, which takes an oblate spheroid shape. This deformation is apparent for millimetric size droplets, presented in Fig. 1*A*, but it is less pronounced for diameters in the range of a few hundred μm, as shown in the top row images from Fig. 1*C*. The curved shape of the reflector helps to concentrate the acoustic wave in the center of the levitator, which generates a radial pressure gradient. This radial gradient is much smaller than in the vertical direction but is sufficient to maintain millimeter sized drops on the vertical axis of the levitator. Nevertheless, droplets which are submillimeter in size can easily move radially. This problem affects measurements at the end of the evaporation process in particular. The droplets were first observed with forward illumination using a Nikon D90 SLR camera and a

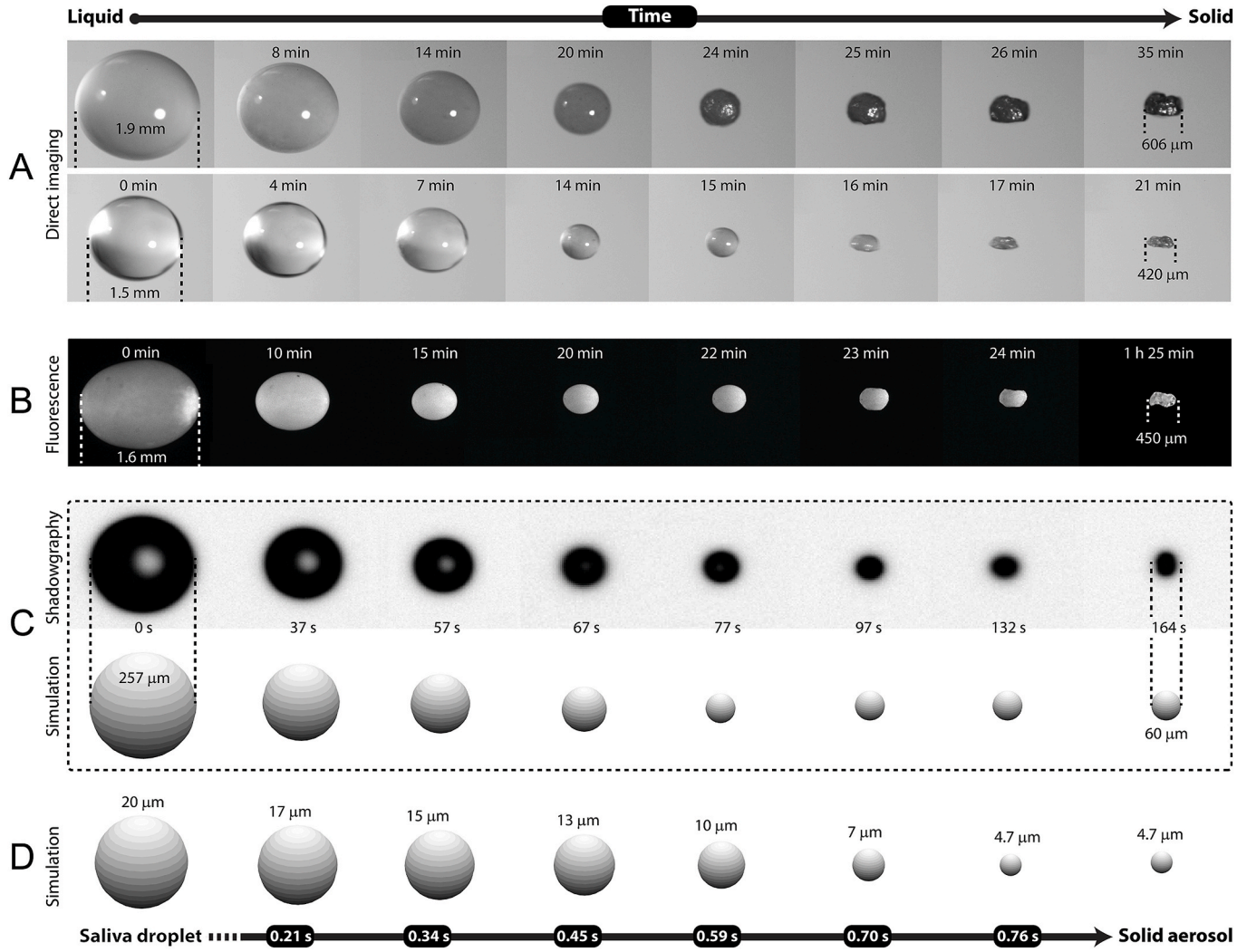

Fig. 1. Evolution of saliva droplets over time showing the transition of individual liquid droplets to solid particles due to the evaporation of their water content. In (*A*) two examples of large droplets are shown, where the solidification of the droplet is clearly visible. A video showing the same process can be seen in Video S1 in the Supplementary Information. In (*B*) some fluorescein dye has been mixed with saliva (at $1 \cdot 10^{-5}$ mol/L) and the droplet was excited at $\lambda = 450$ nm. It shows the induced fluorescence is still detected from the residue, demonstrating that the dye molecules are not evaporating with water. A video showing the solid residue in rotation can be seen in Video S2 in the Supplementary Information. (*C*) is a comparison between shadowgraphy images and simulated results showing a good agreement of droplet evaporation over time. (*D*) is a numerical prediction of a 20 µm droplet transiting down to 4.7 µm within less than a second. In this simulation, the ambient temperature is $T_{amb} = 22°C$ and the relative humidity is $RH = 55\%$ which corresponds to the cases (*C*) and (*A*). However, in (*B*) $T_{amb} = 22°C$ and $RH = 65\%$.

microscope objective resulting in a resolution of 1.1 µm/pixel. In order to ensure that the droplet is perfectly stable, the observations are carried out with droplets having diameters greater than 1 mm (Fig. 1*A*). Although this type of illumination does not provide a clear outline of the droplet, it does allow the structure of the droplet to be observed over time. Saliva droplets produced from two different individuals follow very similar evolutions, with the differences related mainly to the initial size. At the beginning of the evaporation process ($t = 0$ min) the droplet looks completely transparent. As time goes on, some of the water evaporates causing the droplet to wrinkle and become opaque. This transformation is due to the concentration of non-volatile electrolytes, like NaCl salt, reaching their saturation limit and causing crystallization to start inside the droplet. The increase in opacity is observed from the moment the droplet starts to solidify ($t = 23$ min for the top case in Fig. 1 *A*) and $t = 16$ min for the bottom case in Fig. 1 *A*). The formation of a solid skin, which then crushes in on itself under the pressure forces in the levitator, is usually observed for millimeter-size droplets (see the Video S1 in the Supplementary Information). As a result, the shape of the solid residue is non-spherical, contrary to droplets with smaller initial sizes.

Supplementary data related to this article can be found at https://doi.org/10.1016/j.envres.2021.112072.

SARS-COV-2 viruses have a size ranging from 50 nm to 140 nm. To ensure that these particles do not evaporate with the liquid phase experiments using fluorescein have also been performed. For this purpose, the saliva droplet was seeded with fluorescein (approximately 5 Å in size) at a concentration of 10^{-5} mol/L. A fluorescence signal is then induced by exciting the droplet using a laser with a wavelength of λ= 450 nm. This signal was detected through a long path 514 nm filter using a sCMOS Camera (ANDOR Zyla 5) equipped with a telecentric objective (Bi-telecentric lens for 35 mm detectors, magnification: 2×), This optical path results in a pixel resolution of 3.25 µm/pixel. The induced fluorescence was also observed in the final solid residue, which demonstrates that the dye molecules do not evaporate along with the water. Since these molecules are much smaller than the virions, we can assume the virus does not evaporate with the air.

A shadowgraphy configuration was chosen to study the evolution of the droplet diameter over time, as it allows images with sharp droplet contours to be captured. All of the tests conducted were performed for an

ambient temperature of 22°C and a relative humidity of 55%. The evaporation process was recorded using the same detection setup as the fluorescence measurement, with the camera recording images at 1 frame per second. Fig. 1*C* shows an example of shadow images at different evaporation times. Assuming the droplet is an oblate ellipsoid of revolution, the volume equivalent diameter can be computed as $d_{eq} = \left(S_l^2 S_s\right)^{1/3}$ where S_l and S_s are the major and minor axes respectively. The detection of the droplet contour on the images uses an automatic image thresholding algorithm (Bradley and Roth, 2007) which allows the pixels to be separated into two classes, foreground and background. For each experiment, image acquisition is stopped when no variation in the diameter is observed for more than 1 min. Shadowgraphy images are compared with simulated results, and show a good agreement of droplet evaporation over time. Fig. 1*D* presents the simulated evolution of a 20 μm droplet. It shows the saliva transitions from droplet to solid aerosol in less than 1 s.

A typical evolution of the droplet equivalent diameter is presented in Fig. 2. During the evaporation phase, the square diameter of the droplet decreases approximately linearly with time, then stabilizes due to crystallization. The oscillations are due to the movement of the residual solid particle, which is small and irregular in shape. As the particle size shrinks, the acoustic pressure gradient is insufficient to block the movement of the particle in the radial direction or to prevent it from rotating.

2. Modeling of saliva droplet evaporation

In the following, the model used to describe the evolution of a saliva droplet (change in composition, temperature, size reduction) is summarized. The theoretical description of the droplet evaporation is based on the well accepted evaporation model by Abramzon and Sirignano, which was developed for pure liquids (Abramzon and Sirignano, 1989). This approach is extended here to the case of bicomponent NaCl/water droplets. The composition of human saliva is very complex, so to simplify the modeling an assumption has been applied in that all non-volatile components can be assimilated to sodium chloride salt (NaCl) (Wang et al., 2020; Liet al., 2020). The properties of salty water will be considered whenever needed in the calculations related to the liquid phase. Nevertheless, the question of what initial salt content to use that most accurately describes the droplet evaporation remains open.

2.1. Theoretical description of heat and mass transfer

Classically, heat and mass transfer processes in the gas phase surrounding a vaporizing droplet are described using the quasi-steady approximation (Abramzon and Sirignano, 1989; Law, 1975; Sazhin, 2014). Basically, quasi-steadiness means that the distribution of temperature and vapor concentration in the gas phase immediately adjusts to the local boundary conditions and the droplet size at each instant of the evaporation process. A well established expression for the droplet vaporization rate ($\dot{m}_d$) in the frame of the quasi-steady theory is given by:

$$\dot{m}_d = 2\pi r_d D_v \rho_g Sh\ B_M, \quad [1]$$

In this expression, r_d denotes the time-varying droplet radius. D_v is the mass diffusivity of water vapor into air. ρ_g is the density of the air/vapor mixture. The Spalding mass transfer number B_M in Eq. (1) is defined by:

$$B_M = \frac{Y_{v,s} - Y_{v,\infty}}{1 - Y_{v,s}}, \quad [2]$$

where $Y_{v,s}$ and $Y_{v,\infty}$ are the vapor mass fractions at the droplet surface and in the ambient air, respectively. In Eq. (1), the Sherwood number *Sh* describes the mass transfer rate to the droplet and depends on the evaporation conditions. For a quiescent droplet in stagnant air, the evaporation process is limited only by the mass diffusion of the vapor in the air, and the Sherwood number is then equal to 2. When there is relative motion between the droplet and the gas, or an acoustic field, the Sherwood number takes on a more complex expression as explained later. Similar to the mass transfer, the conductive heat flow from the gas to the droplet, Q_g, can be expressed as a function of the Nusselt number, which is a non-dimensional parameter related to the heat transfer rate to the droplet:

$$Q_g = 2\pi r_d \lambda_g Nu\left(T_{amb} - T_{d,s}\right) \quad [3]$$

In this expression, λ_g is the thermal conductivity of gas and T_{amb} the ambiant gas temperature. Inside the droplet, the cooling and the change in liquid composition are driven by thermal and concentration gradients. More or less refined models have been proposed to take into account the heat and mass transfers within a droplet (Sirignano and Edwards, 2000; Sazhin, 2014). To cite only a few, some models have assumed that gradients are controlled only by thermal conduction and mass diffusion in the liquid (Sazhin, 2014). However, for a moving drop, the shear force on the liquid surface causes an internal circulation that enhances the heat and mass transfer. Consideration of this effect has led to models of "effective thermal conductivity" and "effective mass diffusity", where heat and mass diffusion coefficients are artificially increased. Transport equations can be also solved assuming a Hill vortex inside the droplet (Sirignano and Edwards, 2000; Castanet et al., 2011). Presently, the evaporation conditions encountered by the saliva droplets (either in the acoustic levitator or in their motion in ambient air) allow some simplifications in the modelling. According to Fig. 7, a saliva droplet with an initial diameter of 121 μm has a lifetime τ_{vap} of around 45 s, while the heat diffusion from the surface to the center $\tau_h \approx r_{d0}^2/a_l$ is about 34 ms. This indicates a uniform temperature can be assumed, but that it varies in time. The same argument holds for the mass transfer, with the characteristic time inside the droplet $\tau_m \approx r_{d0}^2/D_{ws}$ of about 3.5 s. This is small in comparison to τ_{vap} so the mixing of the salt can also be considered to be instantaneous. Or in other words, the salt concentration will be uniform inside the droplet. For moving droplets, it should be noted that shear forces exerted by the gas flow on the liquid surface can induce an internal liquid circulation which further accelerates the mixing (Abramzon and Sirignano, 1989; Castanet et al., 2011). In the case of acoustic levitation, the presence of an internal liquid flow has also been observed (Zaitoneet al., 2006). It is generated by the gaseous streaming phase (Fig. 3). Based on the above discussion, the rate of change of the droplet temperature T_d can be determined by:

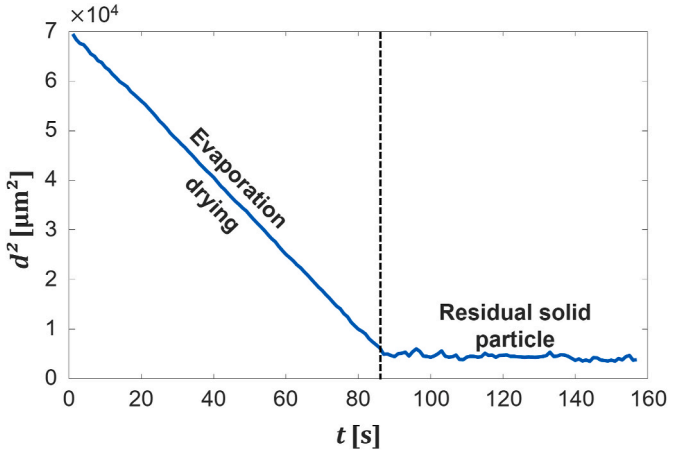

Fig. 2. Evolution of the square of the droplet diameter for the case of Fig. 1C) over time.

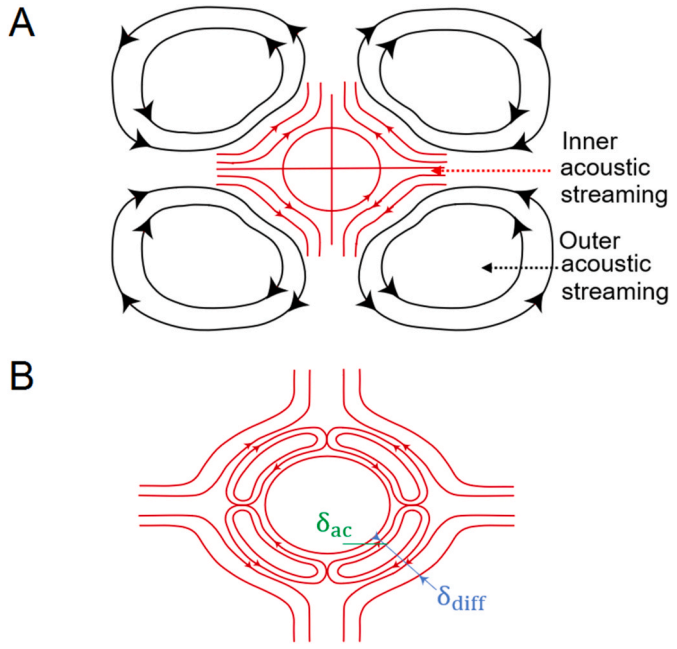

Fig. 3. When an object is placed in an acoustic levitator, the acoustic field generates acoustic streaming around its surface. The inner acoustic streaming is positioned directly at the acoustic boundary layer, whereas the outer acoustic streaming (outer toroidal vortices) surrounds the droplet directly (Yarin et al., 1999). (*A*) outer acoustic streaming. (*B*) inner acoustic streaming, δ_{ac} is the length of the acoustic boundary layer and δ_{diff} is the length of the diffusion boundary layer. Adapted from (Al Zaitone and Tropea, (2011)).

$$m_d \cdot C_{p,l} \frac{dT_d}{dt} = Q_g - L_v \dot{m}_d, \quad [4]$$

where $C_{p,l}$ is the heat capacity of the liquid and T_d is the droplet temperature. Eqs. (1) and (4) are solved numerically using the finite difference method with a time step $dt = 0.01$ s. At each time step of the resolution, the mass of the drop and its temperature are calculated using Eqs. (1) and (4) while updating the values of thermo-physical properties of the gaseous and liquid phase.

The physical properties of the gas phase are evaluated at the reference conditions specified by the 1/3 averaging rule as recommended by Hubbard et al. (1975):

$$\begin{aligned} T_{ref} &= \frac{2}{3}T_s + \frac{1}{3}T_{amb} \\ Y_{v,ref} &= \frac{2}{3}Y_{v,s} + \frac{1}{3}Y_{v,\infty} \end{aligned} \quad [5]$$

Humidity is accounted for a non-null value of $Y_{v,\infty}$ in the expressions of B_M and $Y_{v,ref}$.

As the droplet is vaporizing, the mass of salt remains constant which means that the mass fraction of salt in the liquid Y_{NaCl} can be determined by:

$$Y_{NaCl}(t) = Y_{NaCl,0} \cdot \frac{m_{d,0}}{m_d(t)} \quad [6]$$

where $m_{d,0}$ and Y_{salt_0} are the initial mass of the droplet and initial mass fraction of salt, respectively. The physical properties of the liquid phase (ρ_l, Cp_l …) are updated knowing $Y_{salt}(t)$ and the droplet temperature T_d based on the correlations summarized in the Supplementary Information. To evaluate $Y_{v,s}$, a phase equilibrium is assumed at the liquid/vapor interface. Dissolved salt ions reduce the activity of water and its saturation vapor pressure. This can be expressed by multiplying the saturation pressure of pure water P_{Sat} by the activity coefficient γ_{salt} depending only the mass fraction of salt Y_{NaCl}. The molar fraction of vapor $X_{v,s}$ can be written as:

$$X_{v,s} = \left(1 - X_{NaCl,s}\right) \cdot \gamma_{NaCl} \cdot \frac{P_{Sat}(T_d)}{P}, \quad [7]$$

where $X_{NaCl,s}$ is the molar fraction of salt in the liquid. The curvature of the droplet surface also modifies the equilibrium vapor pressure (Kelvin effect). This phenomenon, which is expected to play a role only for very small droplets (typically less than 1 μm in diameter), can be inserted into the expression of P_{sat} as formulated in the Supplementary Information. The droplet evaporation is finished when the mass-fraction of salt in the droplet reaches the solubility limit of NaCl in water, which corresponds approximately to 357 g/kg (Bharmoria et al., 2012) at 20°C. Interestingly, the solubility of NaCl is rather invariant in the range of temperatures encountered when saliva evaporates in standard ambient air (Bharmoria et al., 2012).

2.2. Effect of acoustic streaming

To complete the model, it is necessary to formulate expressions for the Nusselt and Sherwood numbers. When a drop is moving, heat and mass transfers are accelerated by forced convection. Nusselt and Sherwood numbers of the convective droplet are dependent on the Reynolds number (Re) based on the relative velocity between the droplet and the gas, the droplet diameter and the gas phase properties. Frequently used expressions for *Nu* and *Sh* are provided by the Ranz-Marshall correlation (Ranz and Marshall, 1952):

$$\begin{aligned} Nu &= 2 + 0.6\mathrm{Re}^{1/2}Pr^{1/3} \\ Sh &= 2 + 0.6\mathrm{Re}^{1/2}Sc^{1/3} \end{aligned} \quad [8]$$

where the Reynolds number Re, the Schmidt number *Sc* and the Prandtl number *Pr* are defined by:

$$\mathrm{Re} = \frac{2||v_g - v_\infty r_d}{\nu_g}, \quad Sc = \frac{\nu_g}{D_v}, \quad Pr = \frac{\nu_g}{a_g}$$

The vapor creates a radial flow field called a Stefan flow in the gas surrounding the droplet. This phenomenon is known to reduce the value of the Nusselt and Sherwood numbers when the Spalding number *BM* is large (typically greater than 0.1). Modified expressions for *Nu* and *Sh* involving the Spalding number, can be obtained in the framework of the film theory as proposed by Abramzon and Sirignano (1989).

Acoustic levitation is a useful tool for suspending a drop without contact, but it also introduces some difficulties. One of them is that the acoustic field affects the heat and mass transfer by inducing so-called "acoustic streaming", manifested by the presence of two steady toroidal vortices close to the droplet surface (Fig. 3). In a narrow region of thickness $\delta \sim \sqrt{\nu/\omega}$ close to the droplet surface (inner acoustic streaming), viscous stresses are responsible for a steady streaming motion, which takes the form of a hemispherically symmetric recirculatory flow pattern with closed streamlines. A steady velocity also persists at a larger radial distance from the droplet surface corresponding to the outer acoustic region. An acoustic Reynolds number can be defined on the basis of the velocity amplitude *B* of the gas particle:

$$Re_a = \frac{B^2}{\nu_g\, \omega} \quad [9]$$

where ω the angular frequency of the acoustic streaming. Re_a represents the square of the ratio of the amplitude of the sound wave and the Stokes layer thickness δ (Gopinath and Mills, 1993). As such, it plays a fundamental role in the steady heat and mass transport in the acoustic streaming (Brenn et al., 2007; Yarin et al., 1999). Transport phenomena in the inner acoustic streaming were examined both experimentally and numerically by authors Yarin et al. (1999), Gopinath and Mills (1993). Following their pioneering works, the average Nusselt number *Nu* and the Sherwood number *Sh* can be expressed by:

$$Nu = K\ Re_a \cdot Pr^{\beta}$$
$$Sh = K\ Re_a \cdot Sc^{\beta} \quad [10]$$

In these expressions, K is a parameter that depends on the droplet shape, the droplet displacement relative to the pressure node and the sound pressure level (SPL). According to Yarin et al. (1999) for a small droplet ($r_d \ll \lambda$), the parameter β is equal to 1 and K can be approximated by 1.336, provided that B is calculated from the SPL using the following expression:

$$B = \frac{A_{0e}\sqrt{2}}{\rho_g c_0} \quad [11]$$

$$SPL = 20\ log_{10}(A_{0e}) + 74 \quad [12]$$

where c_0 is the velocity of sound in air and A_{0e} (in dyne/cm^2) is the pressure amplitude of the acoustic wave. Gopinath and Miller (Gopinath and Mills, 1993) proposed $K = 1.413$ and $\beta = 0.667$. The SPL in the acoustic levitator typically ranges between 155 dB and 190 dB, which correspond to $1 < Re_a < 100$ for a sound frequency $f = 58$ kHz. Strictly speaking, Eq. (10) is only valid for $Re_a \gg 1$. In such conditions, the predominant mechanism of transport is the convection by the acoustic streaming. If $Re_a \ll 1$, heat and mass diffusion prevail over convection, and Nu and Sh should in principle take a value of 2. For $Re_a \sim 1$, it is not possible to identify a single dominant mechanism of transport. Nevertheless, experimental results presented by Yarin et al.(Fig. 12 in (Yarin et al., (1999))) suggest that Eq. (10) still provides a reasonably good agreement with experiments when the product $Re_a \cdot Sc$ (and thus $Re_a \cdot Pr$) is as small as 2. As described by (Zaitoneet al., 2006), a certain amount of air flow is required to blow out the outer acoustic streaming; hence a comparison with the theoretical model is possible. The air flow should be strong enough to prevent accumulation of vapor in the outer acoustic streaming, but it should not affect the inner acoustic boundary layer. The same care was adopted in the present study applying a radial blowing of air towards the drop.

2.3. Determination of the initial mass fraction of NaCl

Before the evaporation model can be used, the initial mass concentration of NaCl must be specified. This parameter can be estimated from the observation of the residual size of the dry particles after the droplet vaporization. As a preliminary study, experiments in the ultrasonic levitator were performed on saliva samples from 5 men and 5 women. Approximately 30 saliva droplets were tested per individual with diameters ranging from 120 μm to 300 μm. Fig. 4 shows the values obtained for the ratio between the diameters of the residual particle and the initial droplet, φ. The mean and standard deviation of φ are also displayed in this figure. The average value of all the measurements corresponds to a ratio φ of 0.235 (±0.019). This means that only droplets with a diameter of 21.27 μm or less can be aerosolized (diameter less than 5 μm) and thus remain as a suspension of fine solid particles in the air for long periods of time. There is a slight difference between women and men for this (0.228 ± 0.018 for the men and 0.242 ± 0.019 for the women) but a larger number of individuals would be needed to strengthen this conclusion.

From Eq. (6) it is possible to determine the initial salt mass concentration based on the φ ratio:

$$Y_{NaCl,0}\rho_{l,0} = \varphi^3\ Y_{NaCl,crit}\rho_{l,crit} \quad [13]$$

where $Y_{NaCl,\ crit} = 357$ g/kg and $\rho_{l,crit} = 1290$ kg/m^3 are the maximum mass-fraction of salt and density of the liquid at saturation. Considering the standard deviation of the φ ratio obtained experimentally, which is between 0.19 and 0.27, it can be shown that the initial salt concentration varies between 3.18 g/kg and 9 g/kg. The works of Liu et al. (2017) and Zhang et al. (Zhang, 2011), showed that an initial salt mass fraction of 0.9% allows for a good estimate of the saliva evaporation rate. This value corresponds to the highest value of our experimental results. In view of the large number of experiments carried out here, it seems that an initial salt mass fraction of 6 g/kg is sufficient to reach the average φ ratio.

3. Experimental validation of the numerical model

In a first step, the evaporation model was used to study droplets in acoustic levitation. The first case considered corresponds to an initial droplet size of 121 μm, a relative humidity $RH = 55\%$ and an ambient temperature $T_{amb} = 22°C$.

Fig. 5 shows the evolution of the diameter squared over time for an initial salt concentration of 3 g/kg, 6 g/kg and 9 g/kg. For each case, the simulation is stopped when the maximum mass fraction of salt reaches approximately 357 g/kg (Bharmoria et al., 2012). No differences are observed during the initial phase of evaporation, corresponding approximately to the first 20 s. Then the effect of the salt becomes more important, and different evaporation rates are observed as a function of the initial salt concentration.

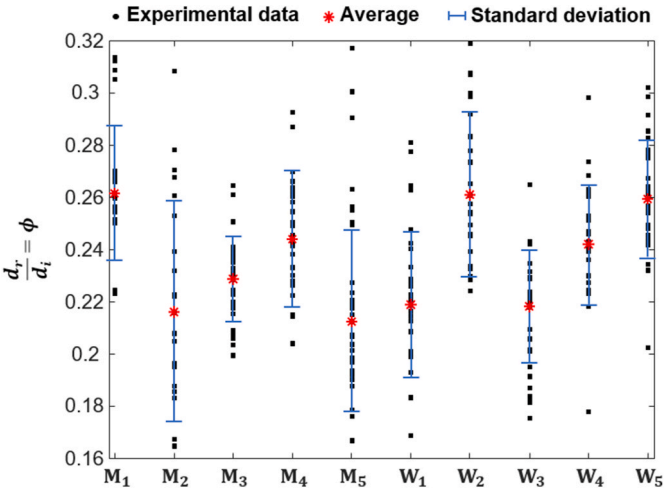

Fig. 4. Evolution of the ratio between the residual diameter d_r and the initial diameter d_i for five men (denoted by M_i) and 5 women (denoted by W_i). The standard deviation obtained from 30 experiments is represented for each case.

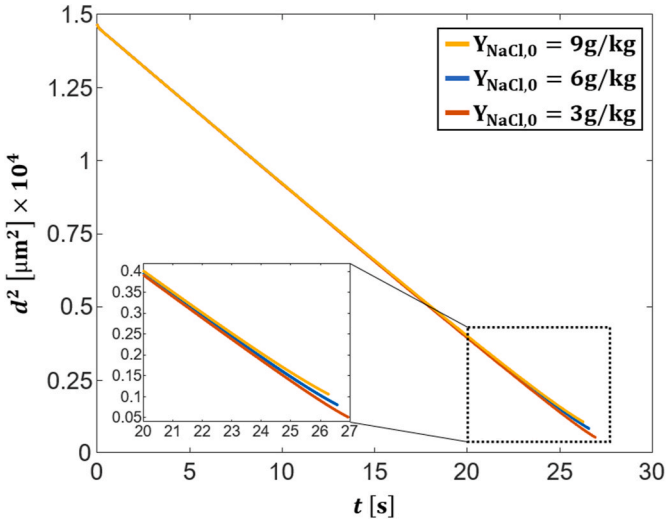

Fig. 5. Time evolution of the square of the droplet diameter, for an initial droplet diameter of 121 μm under a relative humidity of 55%, an ambient temperature of 22°C and an initial mass fraction of salt of 3 g/kg, 6 g/kg and 9 g/kg.

Fig. 6 shows the temporal evolution of the size, temperature, and mass-fraction of salt in the case with an initial diameter of 121 μm, under a relative humidity of 55%, an ambient temperature of 22°C, and an initial mass-fraction of salt of 6 g/kg. After about 2 s, the droplet temperature decreases to 15°C, which is maintained for the majority of the droplet evaporation. This temperature value can be compared to the wet bulb temperature of water. For a pure liquid droplet, in which the temperature converges rigorously to an equilibrium, the wet bulb temperature, depends only the ambient temperature and humidity. Presently, the droplet temperature continues to change with the composition. However, the mass concentration of salt increases very slowly at the beginning of the evaporation process. Thus, the conditions of the d^2-law (constant droplet temperature and composition) are almost satisfied a short time after the introduction of the droplet into the acoustic levitator. Only in the final seconds of the evaporation does the increase in salt concentration accelerate drastically. The result of this composition change is a reduction in the evaporation rate, a noticeable rise in the droplet temperature, and a deviation from the d^2-law, which becomes more pronounced. Law et al. (Law and Law, 1982) have pointed out the existence of a multi-component analogy of the classical d^2-law of droplet evaporation in the case that the droplet concentration distributions remain almost constant during much of the droplet lifetime.

Fig. 7 presents comparisons between numerical and experimental data for different initial droplet sizes assuming an initial concentration of NaCl $Y_{NaCl,0} = 6$ g/kg. As observed, the numerical simulation seems to fit well with the experiments allowing us to validate the initial mass fraction of salt taken. As shown in Fig. 7 the numerical simulations are stopped when the droplet diameter reaches the residual diameter. It is shown in Fig. 4 that the residual diameter was equal to 0.235 times the initial diameter. In the proceeding section, the numerical simulation will take into account this experimental observation in order to better understand virus spreading. An open question is the possibility that the solid residues still contain viruses capable of contamination. In the absence of definitive evidence on this matter, the possibility will be considered in the proposed scenarios of transmission presented here. Thus, an initial salt mass-fraction of 6 g/kg will be used in the following description of droplet motion and evaporation.

4. Transport and evaporation of saliva droplets

4.1. Theoretical description of droplet transport

To determine the potential travel distance of a droplet, and consequently the virus, the evaporation model must include the equations of droplet motion. The air flow generated by a cough must also be specified to evaluate the drag force on the droplets. However, the precise details regarding the flow that is generated by a cough (i.e. jet diameter, velocity profile, turbulence intensities, etc.) are not fully available. Experimental data are generally limited to an area of only a few centimetres, which is not a long enough period to study the droplet evaporation. Recently, Simha et al. (Prasanna Simha and Mohan Rao, 2020) succeeded in characterizing the air velocity during a coughing phase over a distance of 2.5 m using a Schlieren imaging system. They offer the following description of the velocity field, where the axial and transverse distances from the centre of the mouth exit are denoted by x and y respectively:

$$\frac{v_g(x, y=0)}{v_g(x=0, y=0)} = exp\left(\frac{-4.673\, x}{l_c}\right) \quad [14]$$

Here, $v_g(x=0)$ is the initial velocity at the mouth exit, l_c is a fitting parameter expressed in meters (Prasanna Simha and Mohan Rao, 2020), which varies with the coughing conditions. In the case identified by (Prasanna Simha and Mohan Rao, (2020)) as the highest air speed among their measurements, l_c has a value of 3.2 m.

Vansciver et al. (2011) performed a comprehensive study on coughs.

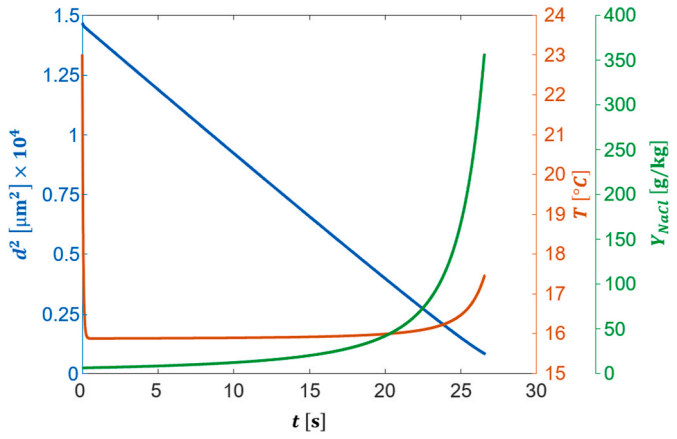

Fig. 6. Numerical example of the time evolution of the square of the droplet diameter, droplet temperature and mass-fraction of salt for a droplet diameter of 121 μm under a relative humidity of 55% and an ambient temperature of 22°C.

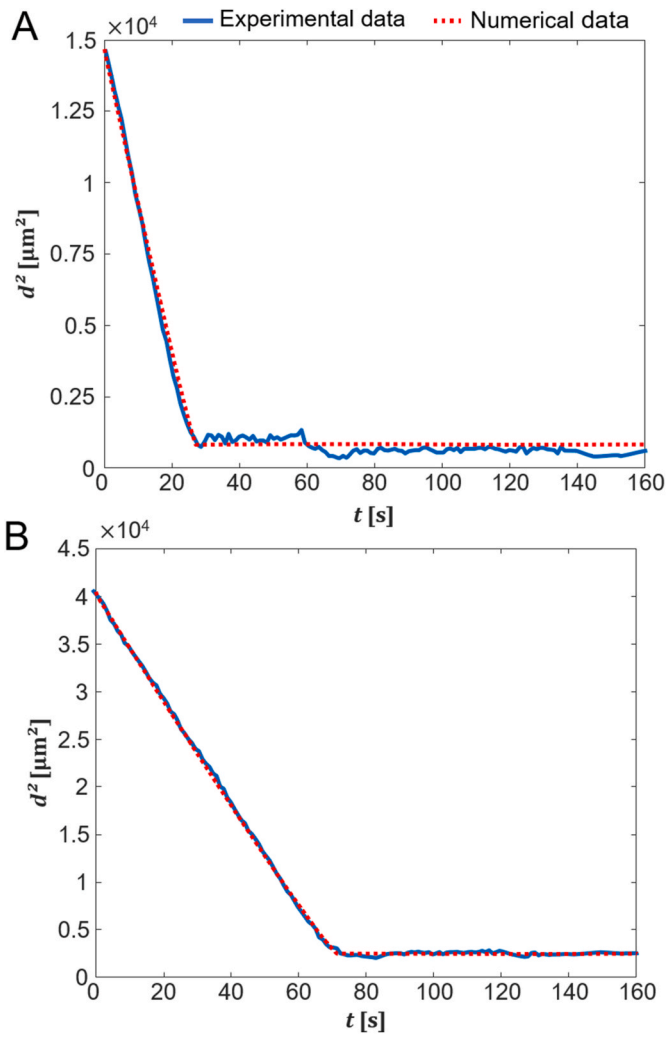

Fig. 7. Comparison between experimental and numerical result of a droplet evaporation under an ambient temperature of 22°C, a relative humidity of 55% and a droplet diameter of (*A*) 121 μm and *B* 201 μm. The numerical simulations are done with the same ambient parameter and an initial SPL ranging from 159 dB to 164 dB.

On average, they show that the flow is a decelerating turbulent round jet that is self-similar with respect to the dimensionless downstream distance, x, given an offset due to the virtual origin (Hinze, 1975):

$$\frac{v_g(y_c)}{v_g(y_c=0)} = 1.003exp(-12.729y_c) \quad [15]$$

where the similarity variable y_c is given by:

$$y_c = \frac{y}{x+0.285} \quad [16]$$

with x the axial distance from the mouth exit and y the position in the transverse direction expressed in meters.

The droplets trajectories can be determined by solving the equation of motion for a droplet subject to gravity and drag force:

$$m_d \frac{d\vec{v_d}}{dt} = -\frac{\pi}{8}\rho_g C_d d^2 ||\vec{v_d} - \vec{v_g}|| (\vec{v_d} - \vec{v_g}) + m_d \vec{g} \quad [17]$$

with m_d the droplet mass, v_d the droplet velocity, ρ_g the air density and d the droplet diameter. C_d is the drag coefficient and is calculated using the Schiller-Naumann correlation (Ellendt et al., 2018):

$$C_d = \begin{cases} \frac{24\left(\left(1+0.15R_e^{0.687}\right)\right)}{R_e} & R_e \leq 1000 \\ 0.44 & R_e > 1000 \end{cases} \quad [18]$$

The solution of Eq. (17) for a particle that does not evaporate, is well known. After a characteristic time $\tau_p \approx \rho_l d^2/18\mu_g$, the particle reaches a terminal velocity dependant on C_d and g. Presently, the largest droplets have a diameter on the order of 100 μm and τ_p is approximately 10^{-2} s. This time is much shorter than the evaporation time, which means that the droplets are always in dynamic equilibrium with the carrier phase. The particles follow the flow rapidly in the x direction but in the y direction they drop at a rate based on their diameter, as seen in Fig. 9.

4.2. Simulation of falling saliva droplets

The first transmission mechanism studied here is the case where drops fall on a surface. This situation is examined by first determining how long it takes for a particle to hit the ground emitted by a person measuring 1.8 m tall. The presence of an ascending airflow will be neglected. and it is assumed that the cough is horizontal and straight, such that the particles fall under the effect of the gravity. Dbouk et al. (Dbouk and Drikakis, 2020) showed that the droplet diameter generated by a cough ranges from 1 to 300 μm with a mean of 86 μm.

Based on that observation, simulations used droplet sizes of 20 μm, 50 μm, 75 μm and 100 μm. Fig. 8 shows the time evolution of the droplet height and size for different initial droplet diameters. The relative humidity, RH, is maintained at 40%, 60% and 80%, and the ambient temperature, T_{amb}, is held at 20°C. As expected, increasing the relative humidity leads to an increase in the evaporation time. For an initial diameter of 75 μm, the evaporation time is about 8.5 s for a relative humidity 40% against 13.6 s for the 60% case. Among the droplets studied, only those with a diameter of 100 μm manage to touch the ground before vaporizing completely and becoming a solid residue. In order to clarify the effects of droplet size, the evaporation times (t_e), and falling times (t_g), were calculated for a range of initial diameters between 15 and 150 μm. The results presented in Fig. 9 correspond to the same conditions as those considered in Fig. 8, namely a relative humidity of 40% and 60%, an ambient temperature of 20°C and a coughing height of 1.8 m. At the intersection between the curves of t_e and t_g, a critical diameter can be defined as (d_{ic}), which corresponds to the smallest initial size for which a droplet can touch the ground before it

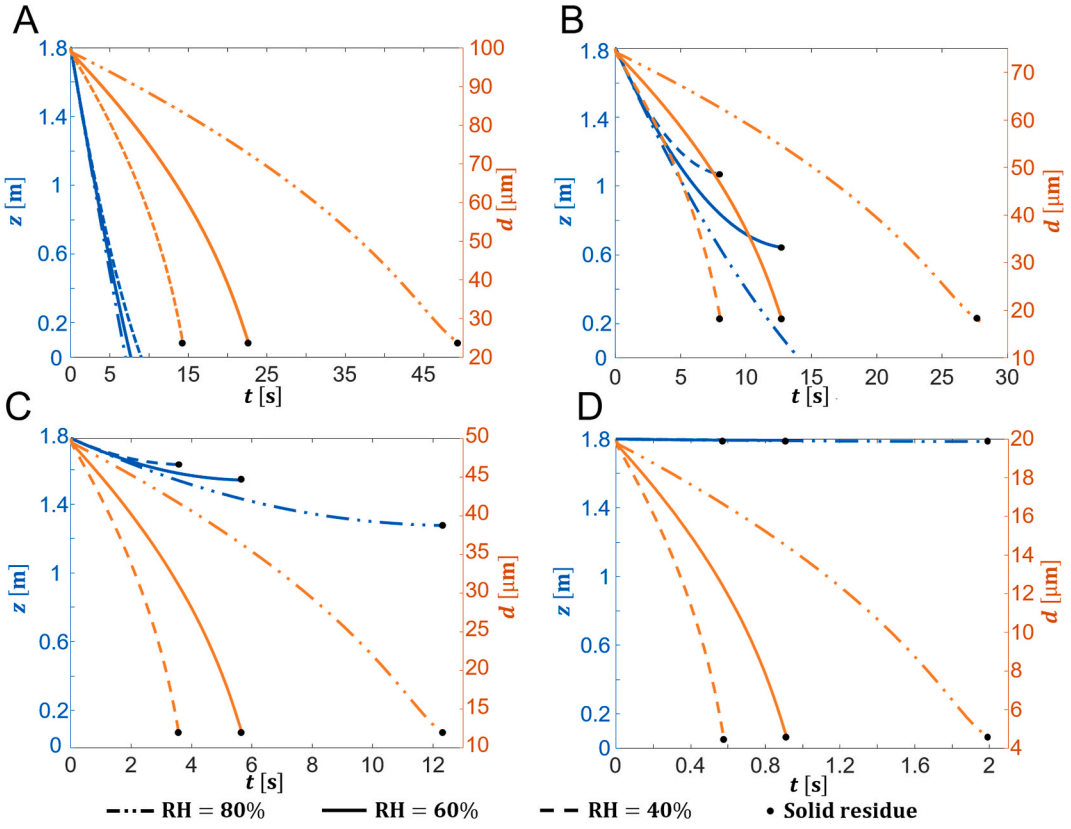

Fig. 8. Evolution of the falling droplet height injected from a human of 1.80 m and of the droplet diameter in function of the time for a initial droplet diameter of (*A*) 100 μm, (*B*) 75 μm, (*C*) 50 μm and (*D*) 20 μm. The droplet initial temperature is 37°C, the ambient temperature is 20°C and the relative humidity is 40%, 60% and 80% respectively.

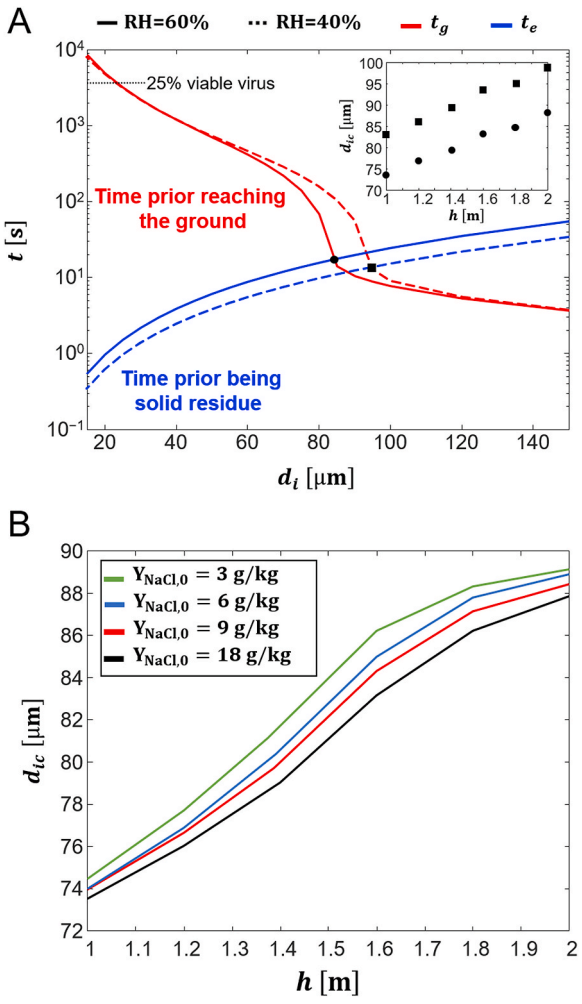

Fig. 9. (*A*) evolution of the airborne lifetime of particles in function of their diameter in the absence of upward air flow under an humidity of $RH = 60\%$ and $RH = 40\%$. The inserted figure represents the critical initial droplet diameter d_{ic} for different initial height (h). (*B*) Evolution of the critical initial droplet diameter d_{ic} in function of the initial salt mass fraction under an humidity of $RH = 60\%$. The effect of the ambient temperature and droplet size can be seen in the Video S4 in the Supplementary Information for a relative humidity of 40%, 60% in Videos S3 and 80% in Video S5.

evaporates. The critical diameter d_{ic} is 84 µm for $RH = 60\%$ and 95 µm for $RH = 40\%$. These values are only valid for a falling height of 1.8 m and an ambient temperature of 20°C. As expected, the sub figure shown in Fig. 9*A* shows that d_{ic} increases with the falling height (h). The effect of the initial mass fraction on the critical diameter is presented in Fig. 9 *B*) and is added the value of 18 g/kg, which corresponds to extremely salty saliva (Tian and Fisk, 2012). According to a study by Doremalen et al. (Van Doremalen et al., 2020), 25% of the virus remains viable in the air after 1 h. Hence, all droplets with an initial diameter greater than the critical diameter have active viral loads when they reach the ground, and could participate in the virus spreading by short term contact. The interactions between the virus and the solid surface will have to be examined more closely to establish the possible duration of the contamination risk (Van Doremalen et al., 2020).Only extremely small drops will exceed this 1 h duration, however droplets that have a diameter smaller than the critical diameter will contribute to airborne spreading.

4.3. Airborne spreading by cough droplets

The virus is also carried by the droplets in the main direction of the cough. As shown in Fig. 9, if the drops are sufficiently small, they can stay in the air for a long time, and retain viable virions for more than an hour. In order to calculate the droplet propagation in this direction, the value of l_c in Eq. (14) must be determined. This value is fixed at 3.2 m which corresponds to the largest velocity observed by (Prasanna Simha and Mohan Rao, (2020)), and is thus the worst case scenario for virus spreading.

Fig. 10 shows the droplets trajectory calculated for different initial droplet sizes, and different ambient conditions (T_{amb} = 20°C and 30°C and RH=40%, 60% and 80%). As expected, the large droplets fall to the ground quickly and are not transported by the air stream over a long axial distance. If we limit the calculations to the formation of the solid grain, it is interesting to note that there is an optimum droplet size that maximizes the transport distance. Droplets which are initially too small evaporate quickly, which reduces the travel distance during evaporation. Fig. 10 for RH=40% and 60% shows that 50 µm droplets are transported the farthest of those studied. This however, does not necessarily mean that this size droplet will spread a pathogen over the widest area since the survival of the virus in the solid residue is unknown. If the virus is able to live long enough in the solid residue, it is the smallest droplets that may well be the greatest vector of contamination, since they will be transported over the longest distances. According to Fig. 9, complete evaporation is achieved in a few seconds, whereas the droplet may remain in suspension for several hours. It is therefore important to study the virus resistance to the conditions encountered in the solid residue that remains at the end of the evaporation process. The role played by the ambient conditions also needs to be considered in this problem. Given that the evaporation rate increases with the ambient temperature, and decreases with the humidity, the distance traveled by the drops before their complete evaporation will change with the environmental conditions. The model presented here is capable of studying the effect these parameters. As shown above, the higher the temperature, and the lower the humidity, the faster the evaporation will take place. Thus, an increase in temperature and a decrease in humidity will be characterized by a shorter spreading distance before the droplets become solid residues. Note that small droplets evaporate very quickly and thus display shorter propagation distances before evaporation compared to larger droplets. For example, under an ambient temperature of 30°C and a relative humidity of 40%, a 20 µm droplet will propagate at a distance of 1.05 m before becoming a solid residue, while a 100 µm droplet will propagate only 0.7 m. Alternatively, for a relative humidity of 80%, small droplets with an initial diameter of 20 µm can reach distances over 3 m before becoming solid residues. Also the solid residue of the droplet with an initial diameter of 20 µm is considered an aerosol ($d < 5$ µm), and would be more likely to contribute to airborne transmission pathways. By considering a higher initial salt mass fraction, this would result in a smaller spreading area of the drops before they become solid residues. On the other hand, considering a lower initial salt fraction would increase the propagation distance.

5. Conclusions

In addition to water, saliva contains non-volatile substances, which are responsible for the formation of a solid particle post evaporation. The evolution of saliva droplets into these crystals has been visualized over time by imaging a single drop suspended in an acoustic levitator. Direct white light illumination was used to document the change of the particle from a liquid into a solid state. Adding a fluorescent dye to the saliva has demonstrated that molecules of ~5 Å are still trapped in the residue even after 1h25min. This observation supports the hypothesis that virions, which are ~100x larger, probably do not escape the evaporation process and remain within the residue. By investigating the saliva droplets from 5 men and 5 women using shadowgraphy imaging, it was found that on average the residual diameter represents 23.5% (±1.8%) of the initial droplet size.

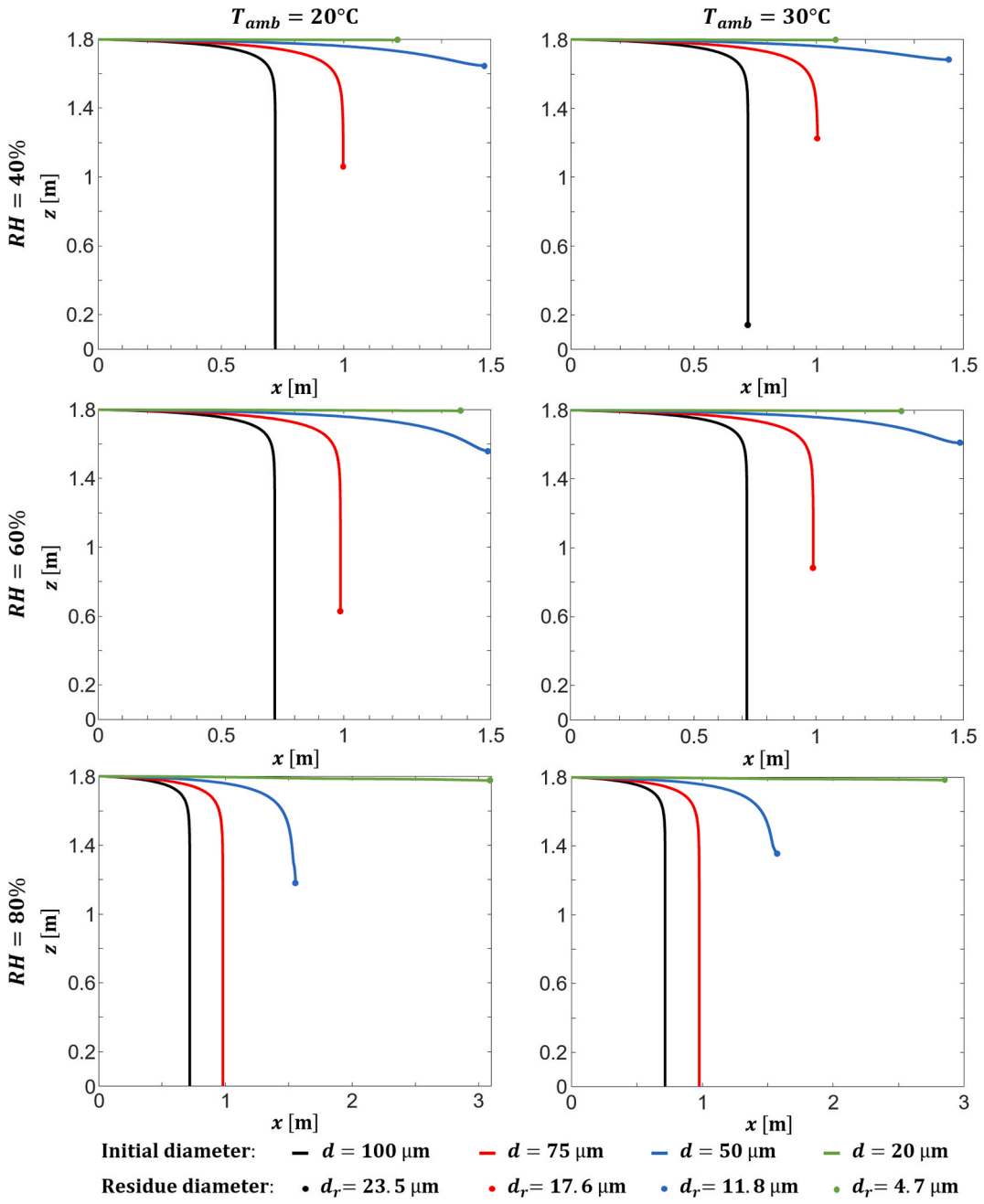

Fig. 10. Evolution of the droplet trajectories for droplet diameters of 20 µm, 50 µm, 75 µm and 100 µm. The droplet trajectories are calculated for three different relative humidities (40%, 60% and 80%) and two different ambient temperatures (30°C and 20°C).

To better understand saliva droplet evaporation and transport phenomena, a numerical model has been developed, validated and applied. This model accounts for the evaporation of a bi-component droplet composed of water and a given mass fraction of salt. A good agreement between the simulated and experimental results were found when an initial salt mass fraction of 6 g/kg was used in the simulation.

The validated model has been employed to deduce the droplet size as a function of time for both the case of falling droplets in air, and that of cough droplets. This work can thus determine which droplet sizes are likely to evaporate into airborne solid residues prior to reaching the ground for relative humidities of 40% and 60% and various injection heights. For the case of a droplet falling from a height of 1.8 m, droplets larger than 85 µm are observed to reach the ground prior to complete evaporation. Additionally, for any realistic ambient condition, droplets smaller than 21 µm will always turn into small solid aerosols within less than a 1 s under a relative humidity of less than 60% and a temperature of 20°C. For the 80% relative humidity case, this process will occur in less than 2 s. As a result, they will hang in the air indefinitely, potentially traveling long distances, and spreading the virus over a wide area.

For the case of cough droplets, simulations have shown that the distance traveled by the droplets prior to becoming solid residues varies greatly with initial size. A 50 µm droplet for example, which evaporates in less than 6 s into a ~12 µm solid particle, is shown to propagate the farthest distance, consistently traveling approximately 1.5 m (for relative humidities lower than 60%). This situation is potentially one of the most dangerous for three reasons:

1) There is a high probability that these residues contain virions due to the fairly large initial droplet volume.

2) The size of the residue remains sufficiently small at ~12 μm that it will remain suspended in the air over a long period of time, and as a consequence, be transported by surrounding flows.
3) This size is also sufficiently large to protect the encapsulated virions from the surrounding environment, preventing exposure to harmful UV light
4) The residue remains at ~90% of its initial ejection height and can potentially be directly inhaled by another person of same height, positioned at 1.5 m.

To conclude, the model presented herein allows for a better understanding of how diseases, such as SARS-CoV-2 and its variants, propagate via airborne and droplet vectors. The data show that droplets with an initial size of 20–50 μm will result to residues which are 4.7–12 μm in size. Those solid residues, which are produced within a few seconds, may present the highest risk for virus spreading. Future work will require combining the evaporation model developed herein with experimental measurements of the initial size and velocity of exhaled respiratory droplets. This approach will help to significantly advance our understanding of COVID-19 transmission via respiratory emissions.

Declaration of competing interest

The authors declare that they have no known competing financial interests or personal relationships that could have appeared to influence the work reported in this paper.

Acknowledgments

The European Research Council (ERC - 638546) and the Swedish Research Council (Vetenskapsrådet 2016–03894) are acknowledged for their financial support. The authors would also like to thanks Dr. Alexander Permogorov for loaning his microscopic imaging device.

Appendix A. Supplementary data

Supplementary data to this article can be found online at https://doi.org/10.1016/j.envres.2021.112072.

Author statement

Mehdi Stiti designed the experiment, developed the numerical model, performed research, analyzed data and wrote the article. Guillaume Castanet developed the numerical model, analyzed data and wrote the article. Andrew Corber and Marcus Alden wrote the article. Edouard Berrocal designed research, performed research and wrote the article.

References

Abramzon, B., Sirignano, W., 1989. Droplet vaporization model for spray combustion calculations. Int. J. Heat Mass Tran. 32, 1605–1618.
Al Zaitone, B Ali, Tropea, C., 2011. Evaporation of pure liquid droplets: comparison of droplet evaporation in an acoustic field versus glass-filament. Chem. Eng. Sci. 66, 3914–3921.
Asadi, S., et al., 2020. The coronavirus pandemic and aerosols : does COVID-19 transmit via expiratory particles ? Aerosol. Sci. Technol. 54, 635–638.
Bharmoria, P., Gupta, H., Mohandas, V., Ghosh, P.K., Kumar, A., 2012. Temperature invariance of nacl solubility in water: inferences from salt–water cluster behavior of nacl, kcl, and nh4cl. J. Phys. Chem. B 116, 11712–11719.
B Blocken, F Malizia, TV Druenen, T Marchal, Towards Aerodynamically Equivalent COVID19 1 . 5 M Social Distancing for Walking and Running. , 1–12 (year?).
Boucher, O., 2015. Atmospheric Aerosols in *Atmospheric Aerosols*. Springer, pp. 9–24.
Bourouiba, L., 2020. Turbulent Gas Clouds and Respiratory Pathogen Emissions Potential Implications for Reducing Transmission of COVID-19, vol. 323, pp. 2020–2021.
Bourouiba, L., Dehandschoewercker, E., Bush, J.W., 2014. Violent expiratory events: on coughing and sneezing. J. Fluid Mech. 745, 537–563.
Bradley, D., Roth, G., 2007. Adaptive thresholding using the integral image. J. Graph. Tool. 12, 13–21.
Brenn, G., Deviprasath, L., Durst, F., Fink, C., 2007. Evaporation of acoustically levitated multi-component liquid droplets. Int. J. Heat Mass Tran. 50, 5073–5086.
Castanet, G., Labergue, A., Lemoine, F., 2011. Internal temperature distributions of interacting and vaporizing droplets. Int. J. Therm. Sci. 50, 1181–1190.
Chaudhuri, S., Basu, S., Kabi, P., Unni, V.R., Saha, A., 2020. Modeling the Role of Respiratory Droplets in Covid-19 Type Pandemics Modeling the Role of Respiratory Droplets in Covid-19 Type Pandemics, 063309.
Czerwiec, T., et al., 2017. Thermal management of metallic surfaces: evaporation of sessile water droplets on polished and patterned stainless steel. In: IOP Conference Series: Materials Science and Engineering, vol. 258. IOP Publishing, 012003.
Dbouk, T., Drikakis, D., 2020. On respiratory droplets and face masks. Phys. Fluids 32.
Ellendt, N., Lumanglas, A., Moqadam, S.I., Mädler, L., 2018. A model for the drag and heat transfer of spheres in the laminar regime at high temperature differences. Int. J. Therm. Sci. 133, 98–105.
Feng, Y., Marchal, T., Sperry, T., Yi, H., 2020. Influence of wind and relative humidity on the social distancing effectiveness to prevent COVID-19 airborne transmission : a numerical study. J. Aerosol Sci. 147, 105585.
Goldman, E., 2020. Exaggerated risk of transmission of covid-19 by fomites. Lancet Infect. Dis. 20, 892–893.
Gopinath, A., Mills, A.F., 1993. Convective heat transfer from a sphere due to acoustic streaming. J. Heat Tran. 115, 332–341.
Gupta, J.K., Lin, C.H., Chen, Q., 2009. Flow dynamics and characterization of a cough. Indoor Air 19, 517–525.
Hinze, J., 1975. Turbulence, "edition, vol. 2. MacGraw Hill, New-York.
Hubbard, G., Denny, V., Mills, A., 1975. Droplet evaporation: effects of transients and variable properties. Int. J. Heat Mass Tran. 18, 1003–1008.
Jayaweera, M., Perera, H., Gunawardana, B., Manatunge, J., 2020. Transmission of Covid-19 Virus by Droplets and Aerosols: A Critical Review on the Unresolved Dichotomy. Environmental research, p. 109819.
JI, Partanen, Jaakko, I., 2013. Partanen *.
Jones, N.R., et al., 2020. Two metres or one: what is the evidence for physical distancing in covid-19? BMJ (Clinical research ed.) 370, m3223.
Law, C.K., 1975. Quasi-steady droplet vaporization theory with property variations. Phys. Fluid. 18, 1426–1432.
Law, C.K., Law, H., 1982. A d2-law for multicomponent droplet vaporization and combustion. AIAA J. 20, 522–527.
Lewis, D., 2020. Is the coronavirus airborne ? Experts can ' t agree 1–5.
Lewis, D., 2021. Covid-19 rarely spreads through surfaces. so why are we still deep cleaning. Nature 590, 26–28.
Lieber, C., Melekidis, S., Koch, R., Bauer, H.J., 2021. Insights into the evaporation characteristics of saliva droplets and aerosols: levitation experiments and numerical modeling. J. Aerosol Sci. 154, 105760.
Li, H., et al., 2020. Dispersion of evaporating cough droplets in tropical outdoor environment. Phys. Fluids 32.
Liljeroos, L., Huiskonen, J.T., Ora, A., Susi, P., Butcher, S.J., 2011. Electron cryotomography of measles virus reveals how matrix protein coats the ribonucleocapsid within intact virions, 108, 18085–18090.
Liu, L., Wei, J., Li, Y., Ooi, A., 2017. Evaporation and dispersion of respiratory droplets from coughing. Indoor Air 27, 179–190.
Liu, Z., et al., 2016. Single fiber optical trapping of a liquid droplet and its application in microresonator. Opt Commun. 381, 371–376.
Páscoa, J.C., 2020. Numerical Modeling of the Distribution of Virus Carrying Saliva Droplets during Sneeze and Cough Numerical Modeling of the Distribution of Virus Carrying Saliva Droplets during Sneeze and Cough, 083305.
Prasanna Simha, P., Mohan Rao, P.S., 2020. Universal trends in human cough airflows at large distances. Phys. Fluids 32.
Prather, K.A., Prather, K.A., Wang, C.C., Schooley, R.T., 2020. Reducing Transmission of SARS-CoV-2. 6197, pp. 1–5.
Ranz, W., Marshall, W., 1952. Evaporation from drops. Chem. Eng. Prog. 48, 141–146.
Roth, A., Stiti, M., Matamis, A., Frantz, D., Richter, M., Alden, M., Berrocal, E., 2021. Analysis of coughed droplets using stereoscopic high-speed imaging. Int. Conf. Liquid Atom. Spray Syst. 1 (1) https://doi.org/10.2218/iclass.2021.6022. In press.
Sazhin, S., 2014. Droplets and Sprays, vol. 345. Springer.
Shao, S., Zhou, D., He, R., Li, J., Zou, S., 2021. Risk assessment of airborne transmission of COVID-19 by asymptomatic individuals under different practical settings. J. Aerosol Sci. 151, 105661.
Sirignano, W.A., Edwards, C.F., 2000. Fluid dynamics and transport of droplets and sprays. J. Fluid Eng. 122, 189–190.
Tian, X., Fisk, I.D., 2012. Salt release from potato crisps. Food & Function 3, 376–380.
SI and others Van Doremalen, Neeltje, Bushmaker, Trenton, Morris, Dylan H., Holbrook, Myndi G., Gamble, Amandine, Williamson, Brandi N., Tamin, Azaibi and Harcourt, Jennifer, L., Thornburg Natalie, J., Gerber, 2020. Aerosol and surface stability of SARS-CoV-2 as compared with SARS-CoV-1. The New England Journal of Medecine 382, 1564–1567.
Vansciver, M., Miller, S., Hertzberg, J., 2011. Particle image velocimetry of human cough. Aerosol. Sci. Technol. 45, 415–422.
Wang, B., Wu, H., Wan, Xf, 2020. Transport and Fate of Human Expiratory Droplets — A Modeling Approach Transport and Fate of Human Expiratory Droplets — A Modeling Approach, 083307.
Yan, J., et al., 2018. Infectious Virus in Exhaled Breath of Symptomatic Seasonal Influenza Cases from a College Community, vol. 115, pp. 4–9.
Yarin, A., Brenn, G., Kastner, O., Rensink, D., Tropea, C., 1999. Evaporation of acoustically levitated droplets. J. Fluid Mech. 399, 151–204.
Zaitone, B., et al., 2006. Evaporation of an acoustically levitated droplet. In: 10th International Conference on Liquid Atomization and Spray Systems. ICLASS, p. 2006.
Zhang, T., 2011. Study on Surface Tension and Evaporation Rate of Human Saliva, Saline, and Water Droplets.